Effects of Structural Parameters and Baffle Patterns on Acoustic Characteristics of Combustion Chamber for Large Diameter LOX/Kerosene Engine *

CAO Chen[1], TAN Yong-hua[2], CHEN Jian-hua[1], LI Long-fei[1]

(1. Science and Technology on Liquid Rocket Engine Laboratory, Xi'an Aerospace Propulsion Institute, Xi'an 710100, China;
2. Academy of Aerospace Propulsion Technology, Xi'an 710100, China)

Abstract: Due to the increase of orbit height and load quality of launch mission, the engine's thrust and diameter of combustion chamber increased, which makes its acoustic oscillation modes more and more complicated. Convergent section of combustion chamber, anti-pulsating baffle and its structural patterns could not only significantly affect the chamber's acoustic characteristics, but also indirectly impact the combustion instability margin. In order to study the effects of structural parameters and baffle patterns on acoustic characteristics, a finite element simulation model of the combustion chamber is established. Firstly, the accuracy of the finite element model is verified by a single nozzle acoustic experiment. On this basis, the influence rules of convergent section of combustion chamber and one hub and six radial baffle are analyzed. The design rationality of baffle patterns for RD-170 and F-1 engine is emphatically investigated in terms of sound pressure distribution. The results show the frequency of 1L and 1T1L mode increases by 14% and 17% , respectively, when convergent section of combustion chamber is considered. For RD-170 engine, the hub baffle locates at the position of 2R mode acoustic velocity anti-node. For F-1 engine, the 13-compartment baffle could not only reduce the radius of 2R mode acoustic velocity anti-node, but also minimize the area of pressure amplitude in tangential modes. The trend of radial vibration mode changing to tangential vibration mode is observed in F-1 engine's combustion chamber with double cross baffle.

Key words: Large diameter combustion chamber; LOX/kerosene rocket engine; Convergent section; Acoustic characteristics; Baffle pattern

CLC number: V434 **Document code**: A **Article number**: 1001-4055(2021)07-1581-12

DOI: 10.13675/j.cnki. tjjs. 200407

大直径液氧煤油发动机燃烧室结构和隔板型式对声学特性的影响

曹 晨[1]，谭永华[2]，陈建华[1]，李龙飞[1]

（1. 西安航天动力研究所 液体火箭发动机技术重点实验室，陕西 西安 710100；
2. 航天推进技术研究院，陕西 西安 710100）

摘 要：随着火箭发射任务轨道高度和载荷质量的提高，发动机推力和燃烧室直径增大，使燃烧室

* 收稿日期：2020-06-01；修订日期：2021-03-12。

作者简介：曹 晨，博士生，研究领域为液体火箭发动机技术。E-mail：18681840502@163.com

通讯作者：谭永华，博士，研究员，研究领域为液体火箭发动机总体技术。E-mail：tanyhcasc@163.com

引用格式：曹 晨，谭永华，陈建华，等. 大直径液氧煤油发动机燃烧室结构和隔板型式对声学特性的影响[J]. 推进技术，2021，42(7)：1581-1592. （CAO Chen，TAN Yong-hua，CHEN Jian-hua，et al. Effects of Structural Parameters and Baffle Patterns on Acoustic Characteristics of Combustion Chamber for Large Diameter LOX/Kerosene Engine [J]. *Journal of Propulsion Technology*，2021，42(7)：1581-1592.）

固有声学振型越发复杂。燃烧室收敛段、抗脉动隔板及其结构型式会显著影响燃烧室的声学特性，进而改变发动机的燃烧不稳定性裕度。为了研究燃烧室结构和隔板型式对声学特性的影响，建立了燃烧室声学有限元模型，并通过单喷嘴声学实验验证了仿真模型的准确性。研究了燃烧室收敛段和一周六径隔板对燃烧室声学特性的影响，重点分析了RD-170和F-1发动机不同隔板型式下燃烧室的声学特性，从声压分布的角度分析了其隔板设计的合理性。结果表明：添加收敛段后，燃烧室的1L和1T1L振型的频率分别提高了14%和17%。RD-170发动机的周向隔板位于2R振型速度波腹位置；F-1发动机所采用的两周八径13分区隔板不仅减小了2R振型速度波腹的半径，而且使切向振型的声压极值面积最小。双十字隔板使F-1发动机燃烧室中出现径向振型切向化的趋势。

关键词：大直径燃烧室；液氧煤油发动机；收敛段；声学特性；隔板型式

1 Introduction

High-frequency combustion instability caused by coupling of pressure pulsation and acoustic vibration modes and its frequency and amplitude of pressure oscillations are consistent with the inherent acoustic modes[1-3]. Due to the increase of the engine's thrust, the diameter of combustion chamber increased, which makes acoustic frequency significantly reduced and the potential risk of combustion instability intensified.

In 1960's, United States developed "Project First" research plan to solve the combustion instability of the Saturn V rocket F-1 engine, about 2000 full scale tests were conducted during the research. Fourteen basic injection patterns in combination with fifteen baffle configurations were tested. Over 90% of the tests conducted during Project First focused on 5U and modified 5U patterns fitted with a 13-compartment by 76.2 mm baffle, finally 13-compartment baffle pattern was chosen as the most optimal structure[4-6].

The RD-0110 engine which operated on a gas generator cycle, was observed high-frequency combustion instability during both development and acceptance testing[7-8]. The high-frequency combustion instability was only observed at engine's start-up stage. Finally, the engine was equipped with several longitudinal felt ribs (made of combustible materials), the high-frequency instability was successfully eliminated. After decades of researches on combustion instability, a large number of experimental results and engineering experience have been summarized[9-10]. However, due to its complicated mechanism, combustion stability of liquid rocket engines is still difficult to effectively predict at present. Compared with controlling the heat release of combustion, it is easier to change the acoustic characteristics of combustion chamber by adding acoustic damping devices such as acoustic cavities, baffles, and half-wavelength injectors. The anti-pulsating baffles are most commonly used to improve combustion stability[11-16], but the influence rules of these devices on acoustic characteristics of combustion chamber still need to be further studied.

China's heavy-lift rocket engine is developing, and this LOX/kerosene staged combustion rocket engine's thrust will be 500 tons[17]. This engine poses a higher challenge to the realization of stable combustion, so it is very necessary to understand the information of combustion stability and systematically take all measures to avoid it[18]. In this paper, three-dimensional finite element modeling and simulation analysis of combustion chambers are carried out based on COMSOL software, in order to study the effects of structural parameters and baffle patterns on acoustic characteristics of combustion chamber for LOX/kerosene engine.

2 Model and Numerical Method

The combustion chamber of LOX/kerosene staged engine is very complex, it's composed of injectors, injector-forming baffles, cylinder section, convergent section, and expansion section of nozzle. As the influencing factors studied in this paper are the diameter of combustion chamber, convergent section, and baffle patterns, the following three simplifications are used for geometric modeling: (1) The effects of injectors and expansion section of nozzle on the acoustic characteristics of combustion chamber are not considered. (2) The injector-forming baffles are simplified as solid baffles. (3) The fluid in combustion chamber model is the uniform gas after combustion. The premises of geometric modeling are the combustion chamber length and fluid state parameters unchanged, the proportional amplification between the diameter of hub baffle, throat diameter and the diameter of combustion chamber.

The acoustic wave equation with no viscosity, no heat loss and no flow are as follows

$$\nabla \cdot \left(-\frac{1}{\rho_0}\left(\nabla p - q\right)\right) + \frac{1}{\rho_0 c^2}\frac{\partial^2 p}{\partial t^2} = Q \tag{1}$$

Where: p is the sound pressure, ρ_0 is the density of fluid medium, q is the dipole sound source, c is the sound speed of fluid medium, Q is the monopole sound source.

Assuming the form of the sound pressure field is $p = p_0 \exp\left[\mathrm{j}(\omega t + \theta)\right]$, substitute p into Eq.(1) to obtain the following Helmholtz equation

$$\nabla \cdot \left(-\frac{1}{\rho_0}\nabla p\right) + \frac{\lambda^2 p}{\rho_0 c^2} = 0 \tag{2}$$

Where: $\lambda = -\mathrm{j}\omega$, the characteristic frequency is $f_0 = \mathrm{imag}(-\lambda)/2\pi$.

Eq.(2) is used to compute the chamber eigenmodes. The model combustion chamber shown in Fig.1 is selected for grid independence verification and the parameters of fluid state are obtained by thermodynamic calculation. Set the sound pressure at injector orifice to zero and the remaining boundary to the wall. The acoustic simulation and experiment parameters of combustion chamber with single injector are shown in Table1. Verification results are shown in Table 2.

The single-injector acoustic experimental system is shown in Fig.2. According to the sound pressure distribution, the sound pressure amplitude of the tangential modes is the largest at the chamber wall, and the radial modes amplitude is the largest at the center. In this experiment, the injector is close to the wall of the combustion chamber, and a loudspeaker is installed on the side wall near the bottom of the combustion chamber to excite oscillation. The loudspeaker is connected to a signal generator, which can generate sound vibrations of different frequencies. Acoustic probes are installed inside the injector, at the exit of the combustion chamber and the side wall of the combustion chamber. The probes can be scanned at any axial, radial, and circumferential position in the combustion chamber to measure the sound field in the experimental combustion chamber. Finally, the acoustic mode is determined by the position of the pitch lines. The verification results are shown in Table 3.

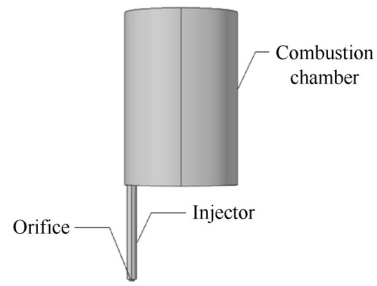

Fig. 1　Configuration of simulation model

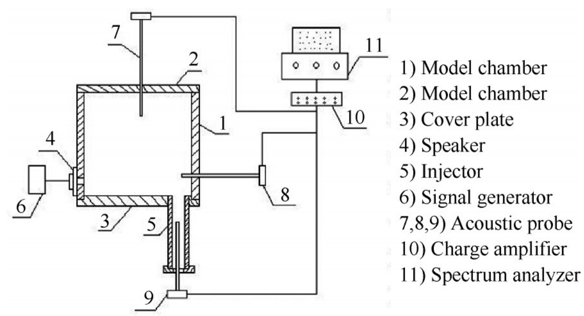

Fig. 2　Single injector acoustic experimental system[19]

Table 1　Parameters of combustion chamber with single injector

Parameter	Value
Chamber diameter/mm	150
Chamber length/mm	220
Sound speed/(m/s)	340
Length of injector /mm	120
Diameter of injector /mm	10

Table 2　Frequency of acoustic modes under different mesh sizes (Hz)

Eigenmode	Mesh size (25mm)	Mesh size (30mm)	Result errors%
1L	783.59	783.59	0
1T1	1326.2	1326.4	0.015
1T2	1332.1	1332.2	7.5×10^{-3}

Table 3　Comparison of simulation results and experimental results (Hz)

Eigenmode	Simulation results	Experimental results	Result errors%
1T1	1326.2	1311	1.16
1T2	1332.1	1378	−3.30

It can be seen from Table 2 that when the mesh size decreases from 30 mm to 25mm, the difference of 1L and 1T mode frequency is no more than 0.02%. Therefore, if the mesh size is not more than 25mm, the convergence and stability of simulation results can be guaranteed. Table 3 shows that the maximum error of acoustic simulation results and experimental results is no more than 3.3%, which proves the validity and accuracy of the numerical calculation method.

The typical acoustic vibration mode of combustion chamber is shown in Fig.3. For 1L mode, the sound pressure gradient only exists in the direction of combustion chamber's axis, and there is only one maximum and one minimum along the axis. In the same way, for 1T mode, the sound pressure gradient only exists in the circumferential direction and there is only one maximum and one minimum. For 1R mode, the sound pressure gradient only exists in the radial direction and there is only one maximum and one minimum. For 1T1L mode, it can be viewed as an overlay of 1T mode and 1L mode. These rules can be extrapolated to identify higher order longitudinal modes.

3 Results and discussion

3.1 Effects of combustion chamber structures on acoustic characteristics

3.1.1 Effects of combustion chamber diameter on acoustic characteristics

Seven different sizes of combustion chamber diameter (280, 330, 380, 430, 460, 510, 560mm) are chosen to analyze the effects of combustion chamber diameter on acoustic characteristics. Boundary conditions are the same as section 2. The finite element model is shown in Fig.4, and Fig.5 show results for 1T, 1R, 1L and 1T1L mode.

With the increase of combustion chamber diameter, the frequency of 1T, 1R and 1T1L mode tends to decline, while the frequency of 1L mode is almost unchanged. The frequency of 1T and 1R mode approximately have an inverse relationship with the diameter of combustion chamber, the accuracy of the numerical simulation method is further verified.

3.1.2 Effects of convergent section of combustion chamber on acoustic characteristics

Add convergent section to the finite element model of combustion chamber, as shown in Fig.6. Grid partitioning and boundary conditions are the same as section 2. The combustion chambers with and without convergent section are compared by simulation, results as shown in Fig.7.

Seen from Fig.7(a) to Fig.7(d), the convergent section of combustion chamber increases the acoustic frequency of all modes. For 1T, 1R and 1T1L mode, the convergent section only changes the size of frequency, but does not change the variation trend of frequency with the diameter of combustion chamber. Fig. 7 (e) shows that convergent section has little effect on the 1T and 1R mode, and the maximum variation range is no

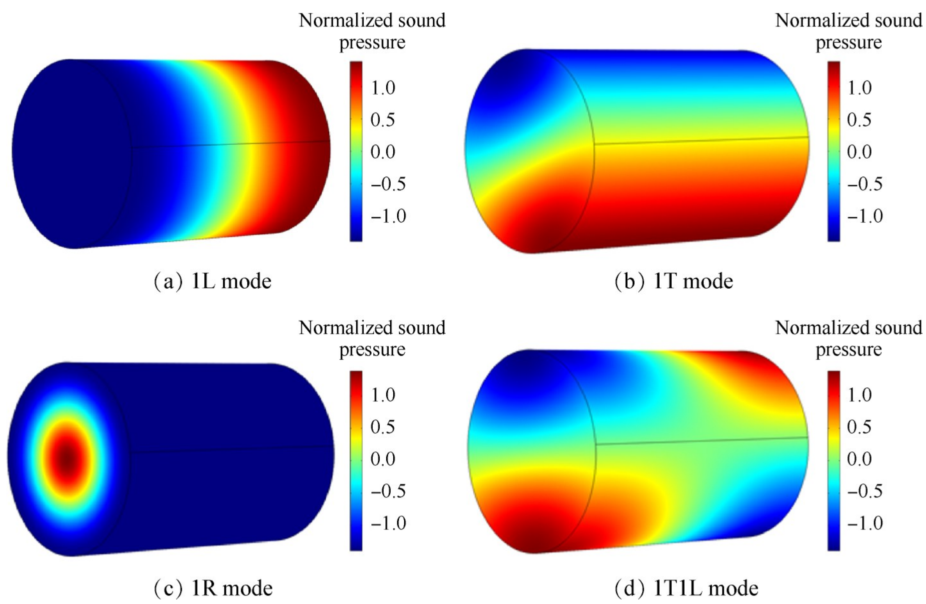

Fig. 3 Sound pressure nephogram of 1L, 1T, 1R and 1T1L mode

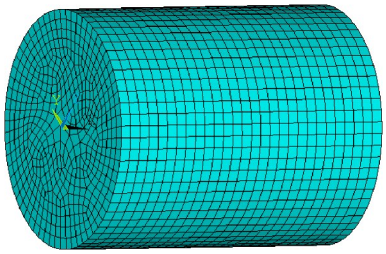

Fig. 4　Configuration of combustion chamber

more than 5%. But the convergent section could significantly affect 1L and 1T1L mode, the maximum variation range is close to 14% and 17%, respectively.

3.1.3　Effects of one hub and six radial baffle on acoustic characteristics

One hub and six radial baffle is added to the finite element model of combustion chamber (as shown in Fig.8), in order to study the effects of baffle on acoustic characteristics for combustion chamber. Boundary conditions are the same as the section 2. The results are shown in Fig.9.

Seen from Fig.9(a) to Fig.9(d), the frequency of 1T, 1R, 1T1L mode reduced by adding one hub and six radial baffle. But the existence of baffle reduces the volume of combustion chamber, so frequency of 1L mode slightly increased. Fig.9(e) shows that one hub and six radial baffle makes a big difference on the frequency for different modes. This kind of baffle has little effect on 1T, 1L and 1T1L mode, the maximum variation range is no more than 6%. The influence of one hub and six radial baffle for 1R mode is greater, the maximum variation range is closed to 30%.

3.2　Effects of baffle patterns on acoustic characteristics

Through the theoretical and experimental study on the combustion stability of F-1 engine and RD-170 engine in the USA and Russia last century, it is found that anti-pulsating baffle is a powerful measure to improve combustion stability for rocket engines. After decades of research, engineers have summarized partial rules of baffle design, mainly divided into the following contents. (1) Hub baffle is designed to suppress the radial oscillations, and radial baffle designed to suppress the tangential oscillations. (2) The optimal design of baffle is at the velocity anti-node position, and the number of baffles is determined by the oscillation modes to be suppressed. (3) For radial high frequency oscillations, the number of hub baffle is equivalent to the order of modes.

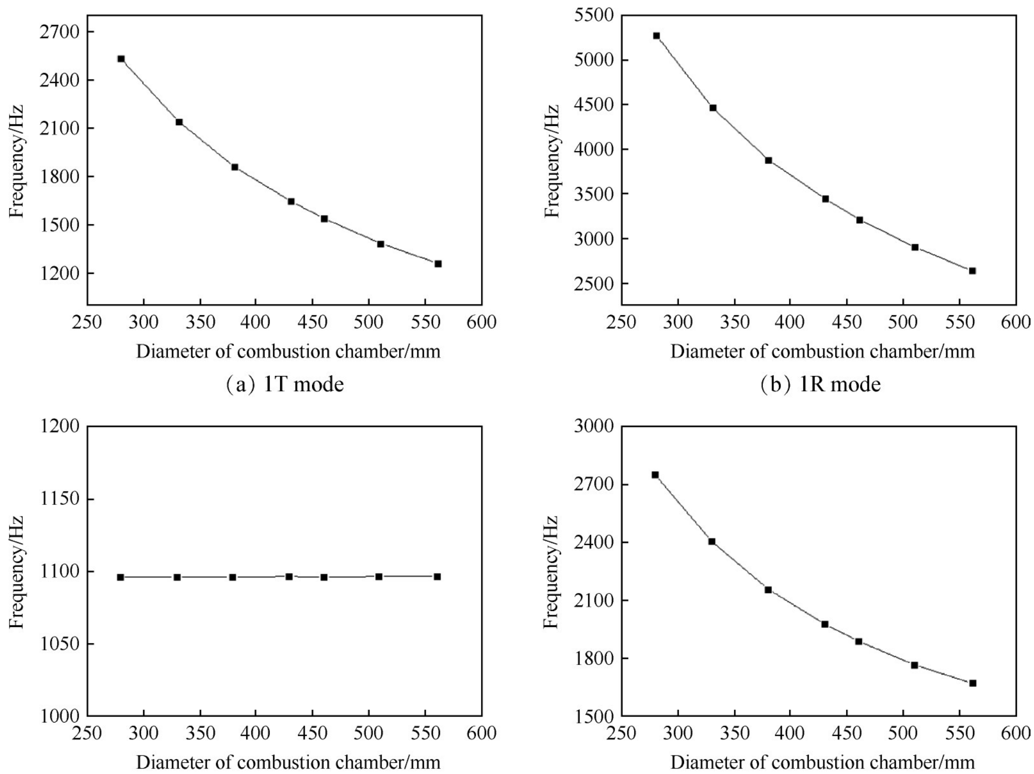

(a) 1T mode　(b) 1R mode

(c) 1L mode　(d) 1T1L mode

Fig. 5　Effects of combustion chamber diameter on combustor frequency

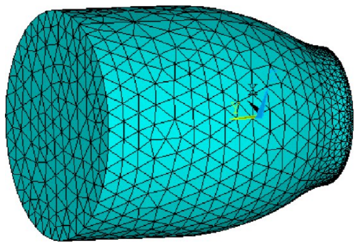

Fig. 6 Finite element model of combustion chamber with convergent section

(4) For tangential high frequency oscillations, the number of radial baffles is more than the order of mode, but better be an odd number. In practical engineering, due to the convenience of processing, the number of radial baffles is usually even.

3.2.1 Effects of baffle patterns on acoustic characteristics for RD-170 engine

RD-170 engine's structural parameters are used as the foundation of geometric modeling, the specific sizes are shown in Table 4. Three types of baffle pattern shown in Fig.10 are selected for simulation. The results of 1T, 1R, 1L and 1T1L mode are shown in Table 5.

Table 5 shows that the influence of hub baffle diameter on the frequency of different modes is quite different. The frequency of 1L mode slightly increased with the increase of hub baffle diameter, the variation range is about 1.5%, but frequency of 1R, 1T and 1T1L mode decreased. The effects of hub baffle diameter on 1R mode are most significant, when the hub baffle diameter

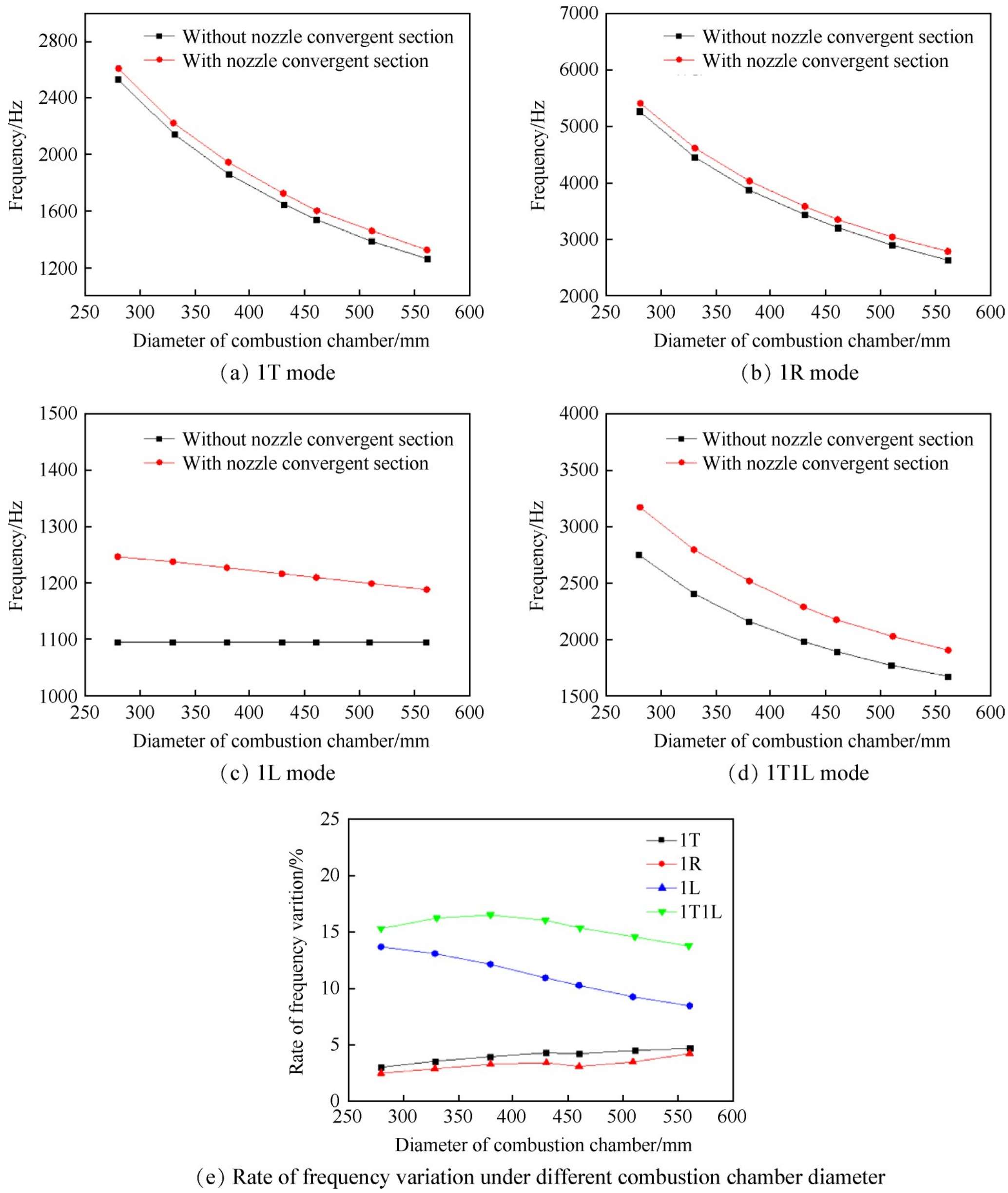

Fig. 7 Effects of convergent section on frequency of combustion chamber

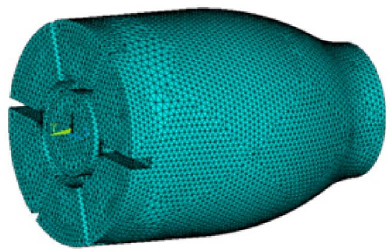

Fig. 8　Finite element model of combustion chamber with one hub and six radial baffle

increased from 0 mm to 180 mm, the frequency dropped by 12.6%.

In order to obtain the rules of hub baffle design, the radial modes should be emphatically studied. Schematic diagram of 1R mode's sound pressure nephogram is shown in Fig. 11. Sound pressure nephogram of 1R mode with different hub baffle diameters are calculated, shown in Fig. 12. Results of 1R mode velocity antinode position with different hub baffle diameters are shown in Table 6.

Table 4　Stractural parameters of RD-170 engine[10]

Parameter	Value
Chamber diameter/mm	380
Throat diameter/mm	235.5
Chamber length/mm	490
Baffle hight/mm	40
Baffle thickness/mm	18.7
Diameter of hub baffle D_h/mm	143

The schematic diagram of 1R mode's sound pres-

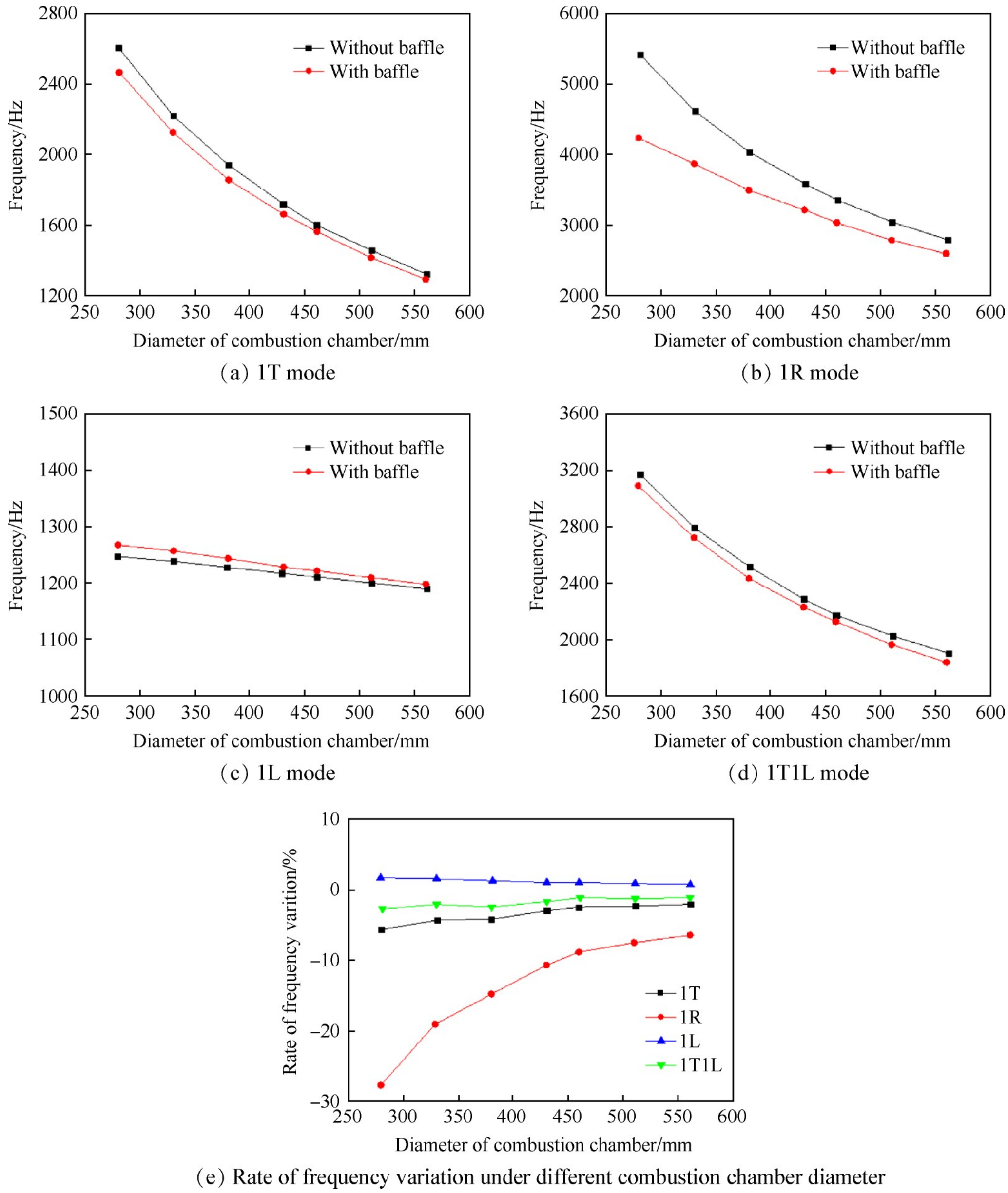

(a) 1T mode

(b) 1R mode

(c) 1L mode

(d) 1T1L mode

(e) Rate of frequency variation under different combustion chamber diameter

Fig. 9　Effects of one hub and six radial baffle on frequency of combustion chamber

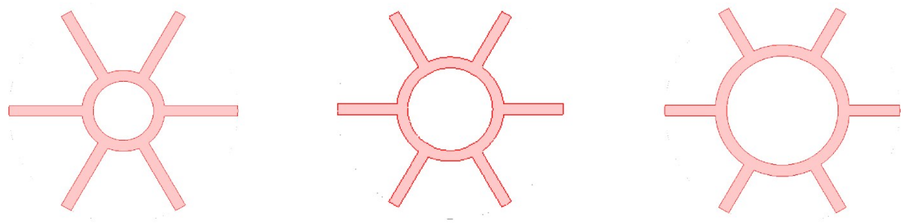

(a) D_h=100mm (b) D_h=143mm (c) D_h=180mm

Fig. 10 Schematic diagram of three types of hub baffle diameter

Table 5 Variation of acoustic frequency under three baffle patterns (%)

Baffle pattern of combustion chamber	Acoustic eigenmodes of combustion chamber			
	1T	1R	1L	1T1L
Without baffle	—	—	—	—
D_h=100mm	-3.5	-6.7	1.5	-1.7
D_h=143mm	-3.1	-10.4	1.51	-1.4
D_h=180mm	-2.5	-12.6	1.53	-1.1

sure nephogram takes shape of concentric circles. Along the radial direction, the sound pressure changes from minimum to maximum. Since the sound pressure changes continuously, so there must be a radius r where the sound pressure turns to zero. According to the relationship between pressure and velocity, the pressure node locates at the position of velocity anti-node. Therefore, the velocity anti-node can be characterized by measuring the contour line position of pressure node.

In Fig.11, r represents the radius of velocity anti-node, R_c is the radius of combustion chamber.

Fig.12 shows that the radius of velocity anti-node is maximum without baffle, the velocity anti-node radius increases as the diameter of hub baffle increases, and the region of extreme acoustic pressure gradually concentrates in the hub baffle. Table 6 shows all three types of hub baffle are not in the position of velocity anti-node, so it can be inferred that RD-170 engine's hub baffle is not set to suppress combustion instability

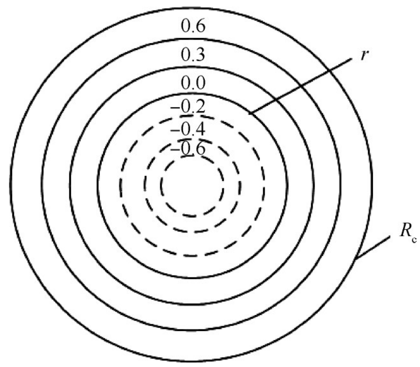

Fig. 11 Schematic diagram of 1R mode sound pressure nephogram

for 1R mode. The smaller diameter of hub baffle makes greater influence on position of 1R mode velocity anti-node. When the diameter of hub baffle is 180 mm, the radius of velocity anti-node is 8.7% less than that without baffle, and when the diameter of hub baffle turns to 100 mm, the ratio turns to 29.2%.

Table 6 Results of 1R mode velocity antinode position with different hub baffle diameters

Baffle pattern of combustion chamber	Relative position of velocity antinode (r/R_c)	Change of velocity antinode position/%
Without baffle	0.6356	-
D_h=100mm	0.45	-29.2
D_h=143mm	0.5535	-12.9
D_h=180mm	0.58	-8.7

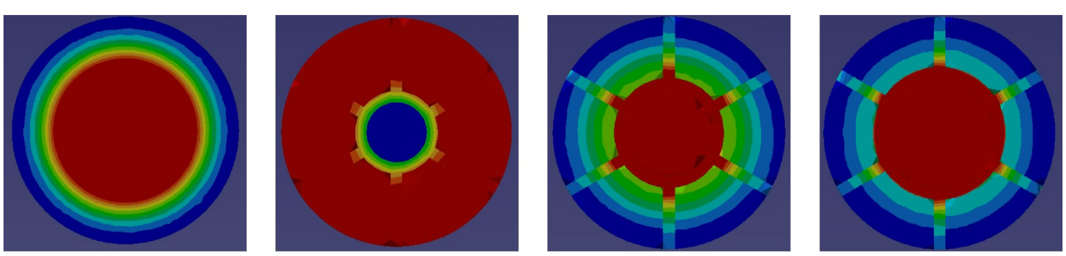

(a) Without baffle (b) D_h=100mm (c) D_h=143mm (d) D_h=180mm

Fig. 12 Sound pressure nephogram of 1R mode with different hub baffle diameters

In order to further analyze the rule of hub baffle design, 2R mode is calculated and the results are shown in Fig.13, 14 and Table 7.

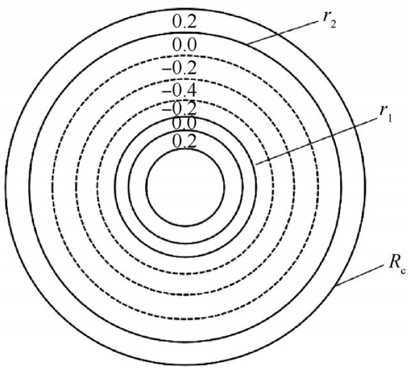

Fig. 13　Schematic diagram of 2R mode sound pressure nephogram

In Fig. 13, r_1 represents the radius of first velocity anti-node, r_2 represents the radius of second velocity anti-node, R_c is the radius of combustion chamber.

Fig. 14 shows a schematic diagram of 2R mode sound pressure nephogram, the same as 1R mode, its shape is concentric circles. However, along the radius direction, the sound pressure changes from maximum to minimum and then from minimum to maximum. It can be seen by Fig.14 and Table 7 that the hub baffle locates at the position of 2R mode acoustic velocity anti-node, the acoustic pressure maximum is completely controlled within the hub baffle area. Therefore, it can be basically inferred that RD-170 engine's hub baffle is set to suppress combustion instability for 2R mode.

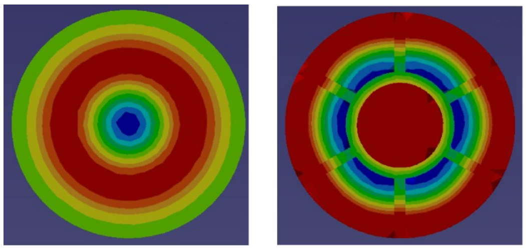

(a) Without baffle　　(b) D_h=143mm

Fig. 14　Sound pressure nephogram of 2R mode with different hub baffle diameters

3.2.2　Effect of baffle patterns on acoustic characteristics for F-1 engine

F-1 engine engine's structural parameters are used as the foundation of geometric modeling, the specific size is shown in Table 8. Four types of baffle as shown in Fig. 15 are selected for simulation. The results of 1T, 1R, 1L and 1T1L mode are shown in Table 9.

Different types of baffles could make a big difference on the effect of acoustic modes. Baffle patterns have little effect on 1T, 1L and 1T1L mode, less than 2%, but have relatively big influence on 1R mode, more than 5%.

It can be obtained from Fig. 16 and Table 10 that four types of baffle have little effect on the distribution of 1R acoustic pressure. Compared with the relative position of velocity anti-node for 1R, the change is less than 1%. Fig. 17 and Table 11 show that four types of baffle have large impact on the distribution of 2R acoustic pressure, double cross baffle and 13-compartment baffle could not only make the relative position of the first velocity anti-node decrease by 18.3%, but also

Table 7　Results of 2R mode velocity antinode position with different hub baffle diameters

Baffle pattern of combustion chamber	Relative position of the first velocity antinode(r_1/R_c)	Diameter of first velocity antinode/mm	Relative position of the second velocity antinode(r_2/R_c)	Diameter of second velocity antinode/mm
Without baffle	0.3487	132.5	0.7919	300.9
D_h=143mm	0.3740	142.0	0.7877	299.3

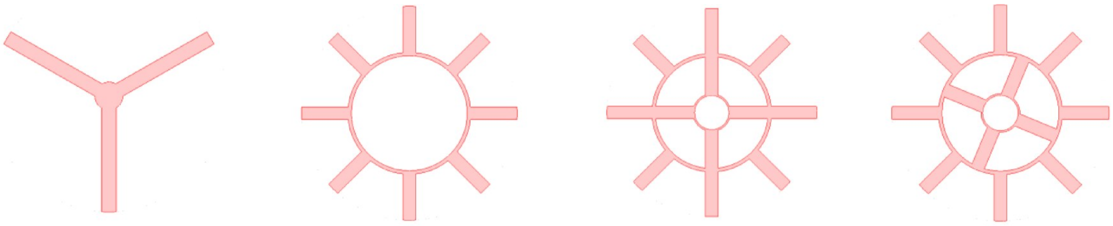

(a) Three radial baffle　(b) One hub and eight radial baffle　(c) Double cross baffle　(d) 13-compartment baffle

Fig. 15　Schematic diagram of four types baffle of F-1 engine

Table 8 Structural parameters of F-1 engine[6]

Parameter	Value
Chamber diameter/mm	1000
Throat diameter/mm	890
Chamber length/mm	1009.39
Baffle height/mm	76.2
Baffle thickness/mm	61
Inner hub baffle diameter D_{hi}/mm	171
Outer hub baffle diameter D_{ho}/mm	553.5

Table 9 Results of four baffle patterns for F-1 engine (%)

Baffle pattern of combustion chamber	Acoustic eigenmodes of combustion chamber			
	1T	1R	1L	1T1L
Without baffle	–	–	–	–
Three radial baffle	−1.4	0.6	0.8	−1.0
One hub and eight radial baffle	−1.0	−5.3	1.3	−0.3
Double cross baffle	−2.0	−4.3	1.7	−0.9
13−compartment baffle	−2.0	−4.4	1.7	−0.9

minimize the area of pressure amplitude on 2R mode. Most importantly, the acoustic pressure distribution of 2R mode is no longer concentric circles.

Table 10 Results of 1R mode velocity antinode position with different types of baffle

Baffle pattern of combustion chamber	Relative position of velocity antinode (r/R_c)	Diameter of velocity antinode/mm
Without baffle	0.6109	610.9
Three radial baffle	0.6140	614.0
One hub and eight radial baffle	0.6040	604.0
Double cross baffle	0.6142	614.2
13−compartment baffle	0.6154	615.4

In order to further analyze the difference of acoustic pressure distribution between double cross baffle and 13−compartment baffle, sound pressure nephogram of 2R and 2T mode with two types of baffle are compared in Fig.18 and Fig.19.

Table 11 Results of 2R mode velocity antinode position with different types of baffle

Baffle pattern of combustion chamber	Relative position of the first velocity antinode(r_1/R_c)	Diameter of first velocity antinode/mm	Relative position of the second velocity antinode(r_2/R_c)	Diameter of second velocity antinode/mm
Without baffle	0.34555	345.55	0.7868	786.8
Three radial baffle	0.3524	352.4	0.7722	772.2
One hub and eight radial baffle	0.3452	345.2	0.7948	794.8
Double cross baffle	0.2873	287.3	0.7979	797.9
13−compartment baffle	0.2824	282.4	0.7730	773.0

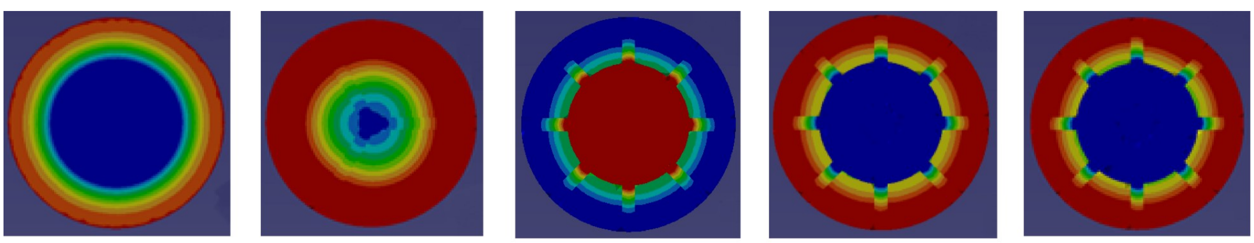

(a) Without baffle (b) Three radial baffle (c) One hub and eight radial baffle (d) Double cross baffle (e) 13-compartment baffle

Fig. 16 Sound pressure nephogram of 1R mode with different types of baffle

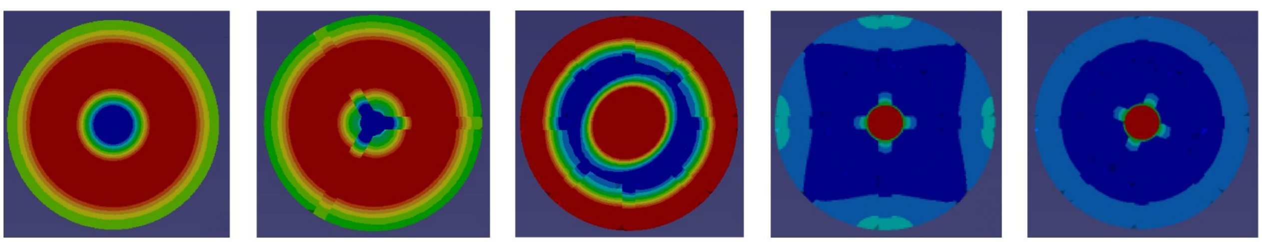

(a) Without baffle (b) Three radial baffle (c) One hub and eight radial baffle (d) Double cross baffle (e) 13-compartment baffle

Fig. 17 Sound pressure nephogram of 2R mode with different types of baffle

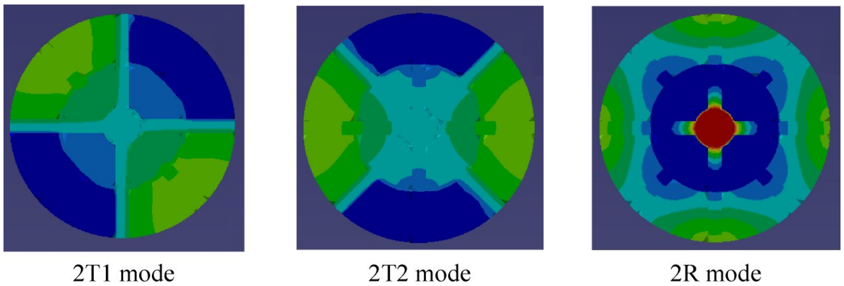

Fig. 18　Sound pressure nephogram of 2T and 2R mode with double cross baffle

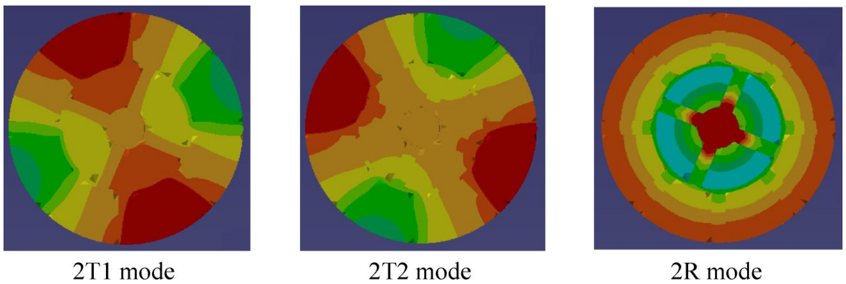

Fig. 19　Sound pressure nephogram of 2T and 2R mode with 13-compartment baffle

It can be seen from the Fig.18 and Fig.19 that the 13-compartment baffle significantly minimizes the area of pressure amplitude on tangential modes in combustion chamber cross section contrast with double cross baffle. And this will improve the combustion stability. According to the 2R mode's sound pressure nephogram, the trend of radial vibration mode to tangential vibration mode appears in combustion chamber with double cross baffle. Under this circumstance, the acoustic pressure distribution of radial mode is no longer concentric circles, and there is sound pressure gradient in the circumferential direction. In the liquid rocket engine, tangential vibration instability is the most serious type of instability, which could destroy the cooling liquid membrane on the inner wall of combustion chamber, strengthen heat transfer between the high temperature gas and inner wall, and then burn up the engine. Therefore, F-1 engine's engineers eventually choose the 13-compartment baffle.

4　Conclusions

Following main conclusions are obtained by studying the acoustic characteristics of combustion chamber:

(1) The acoustic frequency decreases with the increase of combustion chamber diameter, the nozzle convergent section mainly affects the longitudinal mode, and the anti-pulsating baffle mainly affects the transverse vibration mode.

(2) Hub baffle locates at the position of 2R mode acoustic velocity anti-node in RD-170 engine, and the radius of 1R mode acoustic velocity anti-node decreases with the decrease of hub baffle diameter.

(3) For F-1 engine, the 13-compartment baffle could not only reduce the radius of 2R mode acoustic velocity anti-node, but also minimize the area of pressure amplitude on tangential modes. The trend of radial vibration mode to tangential vibration mode appears in combustion chamber with the type of double cross baffle.

(4) Large diameter LOX/kerosene rocket engine, particularly with a diameter of more than 500 mm combustion chamber, requires more complex baffle pattern to inhibit the transverse vibration.

References

[1] Harrje D T, Reardon F H. Liquid Propellant Rocket Combustion Instability[R]. *NASA SP*-194, 1972.

[2] Culick F E C. Stability of High-frequency Pressure Oscillations in Rocket Combustion Chambers[J]. *AIAA Journal*, 2011, 1(5): 1097-1104.

[3] Culick F E C, Yang V. Overview of Combustion Instabilities in Liquid Propellant Rocket Engines[M]. *Reston: American Institute of Aeronautics and Astronautics*, 1995.

[4] Warren D, Langer C. History in the Making-The Mighty F-1 Rocket Engine[R]. *AIAA* 89-2387.

[5] Bostwick L C. Development of LOX/RP-1 Engines for

Saturn/Apollo Launch Vehicles[R]. *AIAA* 68-569.

[6] Oefelin J C, Yang V. Comprehensive Review of Liquid-Propellant Combustion Instabilities in F-1 Engines[J]. *Journal of Propulsion and Power*, 2015, 31(5): 657-677.

[7] You D, Ku D D, Yang V. Acoustic Waves in Baffled Combustion Chamber with Radial and Circumferential Blades[J]. *Journal of Propulsion and Power*, 2013, 29(6): 1453-1467.

[8] Rubinsky V R. Instability Phenomenology and Case Studies: Combustion Instability in the RD-0110 Engine[M]. *Reston*: *American Institute of Aeronautics and Astronautics*, 1995.

[9] Hansen J, Connolly P, Larkin J, et al. Incorporation of RD-180 Failure Response Features in the Atlas V Booster Emergency Detection System[R]. *AIAA* 2011-7120.

[10] Li D, Xu X. Numerical Simulation of Combustion Flow Field in RD-170 Chamber[R]. *AIAA* 2009-4959.

[11] Li D L, Tian Y, Sun J G. Effects of Baffle on Combustion Acoustic Characteristics of Liquid Rocket Engine[J]. *Journal of Aerospace Power*, 2012, 27(3): 715-720.

[12] Kim H J, Lee K J, Choi H S, et al. An Experimental Study on Acoustic Damping Enhancement by the Gap of Baffled Injectors[R]. *AIAA* 2005-4446.

[13] Quinlan J M, Kirkpatrick A T, Milano D, et al. Analytical and Numerical Development of a Baffled Liquid Rocket Combustion Stability Code[J]. *Journal of Propulsion and Power*, 2012, 28(1): 122-131.

[14] You D, Yang V. Linear Stability Analysis of Baffled Combustion Chamber with Radial and Circumferential Blades[R]. *AIAA* 2005-930.

[15] Eversman W, Roy I. The Effect of a Baffle on Acoustic Radiation Directivity[R]. *AIAA* 98-2250.

[16] Quinlan J, Bibik O, Zinn B. Experimental and Numerical Combustion Instability Modes in Asymmetric Baffled Chambers[R]. *AIAA* 2010-6802.

[17] Li Xiang-ning, Liu Yu. Basic Parameters Analysis of First Stage Engine System for Heavy Lift Vehicle[J]. *Journal of Aerospace Power*, 2010, 25(1): 180-186.

[18] Li Long-fei, Chen Jian-hua, Liu Zhan-guo. Control Techniques of High Frequency Combustion Instability for High Thrust LOX/Kerosene Staged Combustion Cycle Engine[J]. *Missiles and Space Vehicles*, 2011(3): 16-19.

[19] CAO Chen, TAN Yong-hua, Chen Jian-hua. Effects of Gas Nozzle and Resonators on Acoustic Characteristics of Combustion Chamber[J]. *Journal of Aerospace Power*, 2019, 34(8): 1836-1846.

（编辑:刘萝威）